JAAS

Novel method for measuring ultra-trace levels of U and Th in Au, Pt, Ir, and W matrices using ICP-QQQ-MS employing an O2 reaction gas

Journal:	*Journal of Analytical Atomic Spectrometry*
Manuscript ID	JA-ART-05-2020-000220.R1
Article Type:	Paper
Date Submitted by the Author:	28-Aug-2020
Complete List of Authors:	Harouaka, Khadouja; Pacific Northwest National Laboratory; Pacific Northwest National Laboratory Hoppe, Eric W ; Pacific Northwest National Laboratory, NSD Arnquist, Isaac; Pacific Northwest National Laboratory

Table 1. Tuning and acquisition parameters applied for the mass shift method. Channels used for analyte and tracer measurements are italicized.

parameter	condition
single quad mode (interference characterization)	
RF power (W)	1600
nebulizer gas (L/min)	0.69
makeup gas (L/min)	0.17
m/z	acq. time (s)
227-239	1.0
replicates	3
sweeps/replicate	10
MS/MS mode[a] (measurement accuracy and detection limit)	
O_2 gas flow (mL/min)	0.38
He gas flow (mL/min)	0
m/z (Q1 → Q2)	acq. time (s)
227 → 227	2.0
228 → 228	2.0
229 → 229	2.0
229 → 245	***15.0***
230 → 230	2.0
231 → 247	5.0
231 → 263	5.0
232 → 232	2.0
232 → 248	***15.0***
233 → 233	2.0
233 → 265	***15.0***
234 → 234	2.0
234 → 250	5.0
234 → 266	5.0
235 → 235	2.0
235 → 251	5.0
235 → 267	5.0
236 → 236	2.0
236 → 252	5.0
236 → 268	5.0
237 → 237	1.0
237 → 253	5.0
237 → 269	5.0
238 → 238	2.0
238 → 270	***15.0***
239 → 239	2.0

a – Reaction gas true flow rate calculated as the product of the fourth cell gas flowrate and the manufacturer provided conversion factor.

Table 2. Inferred polyatomic species detected in the SE solutions in single quad mode.

mass	Interference species
227	$^{197}Au^{14}N^{16}O$, minor Ir and Pt products
228	$^{196}Pt^{16}O_2$, $^{192}Pt^{36}Ar$, $^{193}Ir^{35}Cl$, $^{191}Ir^{37}Cl$
229	$^{194}Pt^{35}Cl$, minor Pt, Ir, and W products
230	$^{194}Pt^{36}Ar$, $^{182}W^{16}O_3$, $^{193}Ir^{37}Cl$
231	$^{191}Ir^{40}Ar$, $^{183}W^{16}O_3$, $^{182}W^{16}O_3H$, $^{195}Pt^{36}Ar$
232	$^{184}W^{16}O_3$, $^{183}W^{16}O_3H$, $^{197}Au^{35}Cl$, $^{192}Pt^{40}Ar$, $^{196}Pt^{36}Ar$
233	$^{193}Ir^{40}Ar$, $^{184}W^{16}O_3H$, $^{197}Au^{36}Ar$
234	$^{194}Pt^{40}Ar$, $^{198}Pt^{36}Ar$, $^{186}W^{16}O_3$
235	$^{195}Pt^{40}Ar$, $^{186}W^{16}O_3H$
236	$^{196}Pt^{40}Ar$, minor W products
237	$^{197}Au^{40}Ar$, minor W products
238	$^{198}Pt^{40}Ar$
239	$^{191}Ir^{16}O_3$

Table 3. Summary of the method accuracy analyses conducted in ME solutions using the natural isotopes of U and Th as the tracer.

sample[a]	^{229}Th (fg·g^{-1})		^{233}U (fg·g^{-1})	
	target	*measured*[b]	*target*	*measured*[b]
blanks				
Sp 0-1	0	0.4 ± 0.4	0	2.6 ± 1.2
Sp 0-2	0	0.1 ± 0.2	0	2.7 ± 0.4
Sp 0-3	0	0.1 ± 0.2	0	4.1 ± 1.7
blank subtracted samples				
Sp 1-1	0.989 ± 0.005	0.7 ± 0.8	1.09 ± 0.01	1.7 ± 1.2
Sp 1-2	1.15 ± 0.01	1.4 ± 0.5	1.26 ± 0.01	2.1 ± 1.3
Sp 1-3	1.14 ± 0.01	0.7 ± 0.9	1.25 ± 0.01	1.6 ± 1.2
Sp 10-1	11.6 ± 0.1	9.6 ± 1.7	12.8 ± 0.1	13.8 ± 1.8
Sp 10-2	11.6 ± 0.1	9.3 ± 1.8	12.8 ± 0.1	13 ± 2
Sp 10-3	11.6 ± 0.1	10.0 ± 1.6	12.8 ± 0.1	14.1 ± 1.8
Sp 100-1	101 ± 1	101 ± 6	101 ± 1	99 ± 4
Sp 100-2	101 ± 1	104 ± 4	101 ± 1	91 ± 3
Sp 100-3	100 ± 1	108 ± 6	100 ± 1	96 ± 4

a –Samples (or Sp) are labeled as Sp-x-y, where ‘x’ is the intended U and Th concentration and ‘y’ is the replicate number

b –The error is the standard deviation of a triplicate measurement

Table 4. U and Th content of various electronic samples as determined using the O_2 mass shift method

sample	replicate	weight (g)	^{232}Th (pg·g^{-1})	LOD (pg·g^{-1})	^{238}U (pg·g^{-1})	LOD (pg·g^{-1})
direct crimp (Axon'Cable)	1	0.3142	35 ± 7	5	41 ± 5	1
	2	0.2945	63 ± 8	6	56 ± 7	1
board mount (Axon'Cable)	1	0.1873	99 ± 10	10	120 ± 11	2
gold bonding wire (Ametek Inc)	1	0.0997	18 ± 14	17	52 ± 6	8
	2	0.2295	27 ± 7	7	190 ± 15	3
	3	0.2572	34 ± 5	7	54 ± 8	3
SQUID arrays (NIST)	1	0.0162	12.8 ± 0.7	1	9.9 ± 1.0	2
	2	0.0173	14.1 ± 0.7	1	8.6 ± 0.9	1
	3	0.0155	19 ± 2	1	15 ± 2	2

Novel method for measuring ultra-trace levels of U and Th in Au, Pt, Ir, and W matrices using ICP-QQQ-MS employing an O_2 reaction gas

Khadouja Harouaka, Eric W. Hoppe, Isaac J. Arnquist

Abstract

Increased demand for improving ultra-low background detection capabilities for rare-event fundamental physics applications has resulted in the need for fast, convenient and clean assay methodologies that either preclude or reduce chemical sample pre-processing. A novel method for the measurement of ultra-trace concentrations (fg·g^{-1} level) of natural ^{232}Th and ^{238}U and non-natural tracer isotopes ^{229}Th and ^{233}U were measured in a solution of 10 µg·g^{-1} each of Au, Pt, Ir, and W in 2% HNO_3 using an ICP-QQQ-MS. Polyatomic interferences across a *m/z* range of 227-239 were characterized: the major interferents with $^{229}Th^+$ is $^{194}Pt^{35}Cl^+$; with $^{232}Th^+$ are $^{184}W^{16}O_3^+$, $^{183}W^{16}O_3H^+$, $^{192}Pt^{40}Ar^+$, $^{196}Pt^{36}Ar^+$, $^{195}Pt^{37}Cl^+$, and $^{197}Au^{35}Cl^+$; with $^{233}U^+$ are $^{193}Ir^{40}Ar^+$, $^{197}Au^{36}Ar^+$, $^{184}W^{16}O_3H^+$; and with $^{238}U^+$ is $^{198}Pt^{40}Ar^+$. Scanning the selected *m/z* range of 227-270 showed that higher oxide polyatomic species from the matrix elements either did not form or did not create significant background on the target analyte masses. All measured concentrations in standard solutions matched the target values within the 98% confidence interval. The Th measurements were 80% accurate or better at the 10 fg·g^{-1} level and above, and the U measurements were 90% accurate or better at the 10 fg·g^{-1} level and above. Measurements at the 1 fg·g^{-1} level were consistent with target values within 1 standard deviation, although the standard deviations of all three replicates were greater than 20% of the measured concentration value. Method detection limits in the matrix solutions were calculated to be 2.74 fg Th and 12.9 fg U. In an electronic sample, which typically have 0.1% precious metal content, our method would give detection limits of 274 fg Th and 1291 fg U given a maximum of 10 µg·g^{-1} coinage metal matrix. This method is but one example of how state of the art quadrupole mass spectrometry and collision reaction cell technology can be leveraged to develop novel analytical capability at ultra-trace levels.

1. Introduction

The advent of commercial *elemental* tandem mass spectrometry (MS/MS) instrumentation has given rise to multiple opportunities for method development aimed at analytes in challenging matrices that either reduce or eliminate the need for extensive sample pre-processing procedures that are both time-consuming and prone to contamination. Such methodologies are of great importance to fundamental high energy and nuclear physics next-generation "rare event" experiments (*e.g.,* dark matter detection, neutrinoless double beta decay, and solar neutrino detection) that require ultra-high purity, low-background detector materials to reach their sensitivity target goals *e.g.,* (1–3). Materials used in detectors undergo high sensitivity assays to accurately model background levels from inherent and/or imparted radiocontamination *e.g.,* (4–10). The main contributors to backgrounds arise from naturally

occurring ^{238}U and ^{232}Th contaminants (the focus of this study) and their progeny, but also ^{40}K and cosmogenic activation products, *e.g.,* ^{60}Co. Typically, the highest sensitivity chemical assays are conducted with inductively coupled plasma mass spectrometry (ICP-MS), which, with meticulous sample preparations and tailored tuning, can measure as low as $fg \cdot g^{-1}$ levels of ^{238}U and ^{232}Th in a variety of materials such as electroformed copper *e.g.,* (10–13).

Some target materials are often comprised of metals that make achieving ultrasensitive measurements using ICP-MS problematic as polyatomic interferences may overlap with the target analyte masses of ^{232}Th and ^{238}U as well as ^{229}Th and ^{233}U that are used as isotope dilution spikes for quantitation of ^{232}Th and ^{238}U. For example, electric contacts, pins, and printed circuit boards (PCBs) in electronic components, metallization on application-specific integrated components (ASICs) and silicon photomultipliers (SiPMs), as well as common resistors, diodes, and superconducting quantum interference device (SQUID) arrays oftentimes contain coinage metals such as Au, Pt, Ir, and W which create polyatomic interferences within the *m/z* range of 227-238 *e.g.,* (14–18).

Polyatomic interferences can sometimes be avoided by diluting the sample sufficiently, applying instrumental tuning strategies (*e.g.,* use of dry or cool plasma), or by removing the offending elements during sample preparations (*e.g.,* via ion exchange chromatography, precipitation, *etc.*). Dilution is typically not viable when attempting to achieve $pg \cdot g^{-1}$ to $fg \cdot g^{-1}$ level measurements as the analyte can be diluted to below detection limits. Chromatographic separations are time-consuming, require a suite of reagents, and are not straightforward for removing Au, Pt, and Ir as they have the same retention as U and Th in most ion exchange resins due to their similar chemical affinities (19–21). While a two-column method could be used for total removal (22), such methods are further time-consuming and create multiple avenues for contamination given the significant effort required for removing backgrounds from ion exchange resins to achieve $fg \cdot g^{-1}$ levels of detection (11). Furthermore, digestions of samples containing these metals often requires the need for HCl or aqua regia, which can produce increased Th

and U background when introduced to the ion exchange resin, even in trace quantities, and/or create matrices with insufficient resin affinity. Furthermore, the use of HCl and HCl containing acids is also the source of chloride polyatomic species that overlap with the target analytes. Minimizing sample preparation procedures is critical for eliminating sources of contamination and increasing sample throughput.

To overcome these challenges, we instead developed a mass shift method where an O_2 reaction gas is reacted with ^{233}U, ^{238}U, ^{229}Th, and ^{232}Th to form monoxide (at *m/z* 245, 248, 249, and 254) and/or dioxide species (at *m/z* 261, 264, 265, 270). The synthetic isotopes of ^{233}U and ^{229}Th in the tracer (at *m/z* 245 and 261 for the single and dioxide of Th, and *m/z* 249 and 265 for the monoxide and dioxide of U, respectively) are used to quantify the oxides of the natural ^{238}U and ^{232}Th in the sample following standard isotope dilution methods.

2. Experimental

2.1 Reagents and labware

Optima grade HNO_3 (Fisher Scientific; Pittsburgh, PA) and 18.2 MΩ·cm deionized water was used to make all reagents used in this study. Elemental standards from HPS (North Charleston, SC) and Inorganic Ventures (Christiansburg, VA) were used to make the matrix solutions. The single element (SE) standards used were 1000 $\mu g \cdot g^{-1}$ each of Au in 2% HNO_3, Pt in 5% HCl, Ir in 2% HCl, and W in 2% HNO_3 and 1% HF. The standard solutions were prepared gravimetrically by diluting the 1000 $\mu g \cdot g^{-1}$ stock to 10 $\mu g \cdot g^{-1}$ with 2% HNO_3. Laboratory work was conducted in a class 10000 cleanroom located at Pacific Northwest National Laboratory (Richland WA, USA).

In order to ensure cleanliness and achieve ultralow background detection limits for Th and U, PFA vials (Savillex, Eden Prairie, MN) were used both for sample digestions, dilutions, and as autosampler vials. Vials were initially cleaned by subsequent leaching in 25% HCl and 40% HNO_3 overnight at 80°C. The vials were validated by adding 1.8 mL of 5% HNO_3 to each vial, allowing them to leach overnight at 80°C, and

then measuring the natural and synthetic Th and U background in the leachate. Vials were considered suitable for use in this study when the measured leachate solutions were at background levels for pure 5% HNO_3 blanks.

2.2 Instrumentation

An Agilent 8900 inductively coupled plasma triple quadrupole mass spectrometer (ICP-QQQ-MS; Agilent Technologies, Santa Clara, CA, USA) with integrated autosampler, Ni skimmer and sampler cones, s-lens, and a standard electron multiplier detector was used for all measurements conducted in this study. The instrument was equipped with a quartz double-pass spray chamber and a 100 $\mu L \cdot min^{-1}$ microflow PFA nebulizer (Elemental Scientific, Omaha, NE, USA). The tuning parameters for optimal signal sensitivity and stability were first determined in single quad mode by tuning the mass analyzer and ion optics with a 0.1 $ng \cdot g^{-1}$ ^{205}Tl standard. The instrument was then switched to MS/MS mode with O_2 gas enabled, and the ion optics and collision cell parameters were refined for maximum oxide generation by observing the relative signals of YO and Y (at *m/z* 105 and 89) and of CeO and Ce (at *m/z* of 156 and 140) in a 0.1 $ng \cdot g^{-1}$ standard. Once optimized, a 500 $fg \cdot g^{-1}$ solution of natural ^{238}U and ^{232}Th was used to double-check the maximum sensitivity of both the monoxide and dioxide product species. All *m/z* collected in single quad mode had 1 second integration times. The selected *m/z* collected in MS/MS mode capture both the highest sensitivity analyte species of UO_2 and ThO. Additional *m/z* were selected in order to monitor for overlapping polyatomic interferences and their oxides in the range of the U and Th analytes. Sample acquisition times varied by the signal intensity at a given *m/z* to ensure higher quality measurements; 15 s was allotted to the target analytes UO_2 and ThO, 5 s was allotted to the *m/z* of the oxides of the polyatomics that directly interfere with the target analytes, and 1-2 s was allotted to the *m/z* of the unreacted polyatomics. A summary of the instrumental parameters is described in Table 1.

Table 1. Tuning and acquisition parameters applied for the mass shift method. Channels used for the analyte and tracer are italicized.

parameter	condition

single quad mode (interference characterization)

RF power (W)	1600
nebulizer gas (L/min)	0.69
makeup gas (L/min)	0.17
m/z	acq. time (s)
227-239	1.0
replicates	3
sweeps/replicate	10

MS/MS mode[a] (measurement accuracy and detection limit)

O_2 gas flow (mL/min)	0.38
He gas flow (mL/min)	0
m/z (Q1 → Q2)	acq. time (s)
227 → 227	2.0
228 → 228	2.0
229 → 229	2.0
229 → 245	***15.0***
230 → 230	2.0
231 → 247	5.0
231 → 263	5.0
232 → 232	2.0
232 → 248	***15.0***
233 → 233	2.0
233 → 265	***15.0***
234 → 234	2.0
234 → 250	5.0
234 → 266	5.0
235 → 235	2.0
235 → 251	5.0
235 → 267	5.0
236 → 236	2.0
236 → 252	5.0
236 → 268	5.0
237 → 237	1.0
237 → 253	5.0
237 → 269	5.0
238 → 238	2.0
238 → 270	***15.0***
239 → 239	2.0

a – Reaction gas true flow rate calculated as the product of the fourth cell gas flowrate and the manufacturer provided conversion factor.

2.3 Determination of interference species, method accuracy, and detection limits

A stock multi-element standard solution (ME solution) containing 10 $\mu g \cdot g^{-1}$ of Au, Pt, Ir, and W was prepared from single element ICP standards. Single element 10 $\mu g \cdot g^{-1}$ stock solutions (SE solutions) of the same elements were also prepared. In order to characterize the matrix-derived polyatomic interfering species, both the 10 $\mu g \cdot g^{-1}$ ME and SE solutions were measured individually in single quad mode by scanning across *m/z* from 227 to 239. A series of ME solutions at 0.1, 1, 5, and 10 $\mu g \cdot g^{-1}$ were measured to determine the signal sensitivity of the polyatomic species as well as the required washout time. In the end, 10 $\mu g \cdot g^{-1}$ was selected as the maximum concentration for our experiments in order to ensure a high enough signal such that all polyatomic species formed could be detected but also low enough in concentration to not cause significant detriment to the instrument (*e.g.,* coating cones/optics, long carryover).

Measurement accuracy and method detection limits were determined by spiking the 10 $\mu g \cdot g^{-1}$ ME solution with a known amount of non-natural ^{233}U and ^{229}Th as isotope dilution tracers and using the natural ^{238}U and ^{232}Th inherent in the ME solution as the spike for isotope dilution quantitation. This method was selected given the expectation that the standard solutions would have natural ^{238}U and ^{232}Th well above the $fg \cdot g^{-1}$ concentration levels we wished to interrogate, which was confirmed through measurement as the ME solution had 3.06 ± 0.05 and 1.60 ± 0.03 $pg \cdot g^{-1}$ for ^{232}Th and ^{238}U, respectively (error is 1SD, n=3) after verifying that the polyatomic interferences were sufficiently avoided with the mass shift method. A portion of the stock ME solution was spiked with 100 $fg \cdot g^{-1}$ of ^{229}Th and ^{233}U tracer and was measured in triplicate in order to quantify the concentration of natural ^{232}Th and ^{238}U inherent to the ME stock. Quantitation followed the standard isotope dilution method (Eqn. 1).

$$C_{analyte} = \frac{I_{analyte} C_{tracer}}{I_{tracer}} \quad \text{Eqn. 1}$$

Here, 'C' is the concentration and 'I' is the measured signal intensity of the oxide of the analyte and tracer isotope. Once determined with the aforementioned high degree of certainty, the concentration of

the ^{238}U and ^{232}Th in the ME solution was used to quantify the synthetic ^{233}U and ^{229}Th in subsequent experiments described below.

Method accuracy was determined by comparing the measured concentration of ^{233}U and ^{229}Th with the known value in a series of prepared samples. The samples were prepared in triplicate, by spiking the 10 $\mu g \cdot g^{-1}$ ME solution with 1, 10, and 100 $fg \cdot g^{-1}$ of synthetic ^{233}U and ^{229}Th gravimetrically. Solutions not containing synthetic ^{233}U and ^{229}Th were used as blanks to determine the detection limits. The limit of detection (LOD) was calculated as 3 times the standard deviation of the triplicate measurement of the blanks (23). Measurement accuracy is determined simply by comparing the blank subtracted concentration measurements with the target value following Eqn. 2.

$$\%acc = 100 \cdot (1 - |\frac{C_m - C_t}{C_t}|) \quad \text{Eqn. 2}$$

Where C_m is the blank subtracted measured concentration and C_t is the target concentration. The 95% and 98% confidence intervals for the triplicate measurements were also calculated and compared with the target values.

3. Results and Discussion

3.1 Interference characterizations

The background contribution from matrix elements across the *m/z* range of 227 to 239 in single quad mode is shown in Figure 1. The intensity of the background interferences on *m/z* 229, 232, 233 and 238 range from 100 to 15000 cps. The sum of the backgrounds from the SE solutions is in good agreement with the background signal of the ME solution, indicating that the formation of the interferences species is not significantly affected by the presence of the other metal ions in the matrix.

The identity of the interferences was deduced by determining the major products formed from each matrix element using the SE standards. In most cases, the product species can be inferred from the mass of the interference and by comparing the ratio of the signal of the isotopes with the natural isotopic abundances of the matrix species. Given the known matrix components, the major inferred

interference species, which are arbitrarily defined for identification purposes as species that form at an intensity greater than 100 cps, are listed in Table 2. The determination of these interferences was not always straightforward in cases where there is multiple overlap between polyatomic species (especially with respect to oxides and hydrides). In these cases, the combined signal of what are likely to be several minor products produce a detectable signal that can be significant (*i.e.,* 100 cps or greater). It is important to consider the characterization of interferences to at least these levels (100 cps) given that typical sensitivities in ultra-trace measurements can reach around 2000 cps/pg·g^{-1} for U and Th in our instrument.

Table 2. Inferred polyatomic species detected in the SE solutions in single quad mode.

mass	Interference species
227	$^{197}Au^{14}N^{16}O$, minor Ir and Pt products
228	$^{196}Pt^{16}O_2$, $^{192}Pt^{36}Ar$, $^{193}Ir^{35}Cl$, $^{191}Ir^{37}Cl$
229	$^{194}Pt^{35}Cl$, minor Pt, Ir, and W products
230	$^{194}Pt^{36}Ar$, $^{182}W^{16}O_3$, $^{193}Ir^{37}Cl$
231	$^{191}Ir^{40}Ar$, $^{183}W^{16}O_3$, $^{182}W^{16}O_3H$, $^{195}Pt^{36}Ar$
232	$^{184}W^{16}O_3$, $^{183}W^{16}O_3H$, $^{197}Au^{35}Cl$, $^{192}Pt^{40}Ar$, $^{196}Pt^{36}Ar$
233	$^{193}Ir^{40}Ar$, $^{184}W^{16}O_3H$, $^{197}Au^{36}Ar$
234	$^{194}Pt^{40}Ar$, $^{198}Pt^{36}Ar$, $^{186}W^{16}O_3$
235	$^{195}Pt^{40}Ar$, $^{186}W^{16}O_3H$
236	$^{196}Pt^{40}Ar$, minor W products
237	$^{197}Au^{40}Ar$, minor W products
238	$^{198}Pt^{40}Ar$
239	$^{191}Ir^{16}O_3$

With respect to the mass range relevant to the analysis of U and Th, the major interferents with ^{229}Th are $^{194}Pt^{35}Cl$; with ^{232}Th are $^{184}W^{16}O_3$, $^{183}W^{16}O_3H$, $^{192}Pt^{40}Ar$, $^{196}Pt^{36}Ar$, $^{195}Pt^{37}Cl$, and $^{197}Au^{35}Cl$; with ^{233}U are $^{193}Ir^{40}Ar$, $^{197}Au^{36}Ar$, $^{184}W^{16}O_3H$; and with ^{238}U is $^{198}Pt^{40}Ar$. Minor overlapping species may include IrO_2 and

their hydrides, PtO_2 and their hydrides, PtNO, and PtCl, as well as WNO, WFO, and WO_3H_2 across the *m/z* range of 227-238.

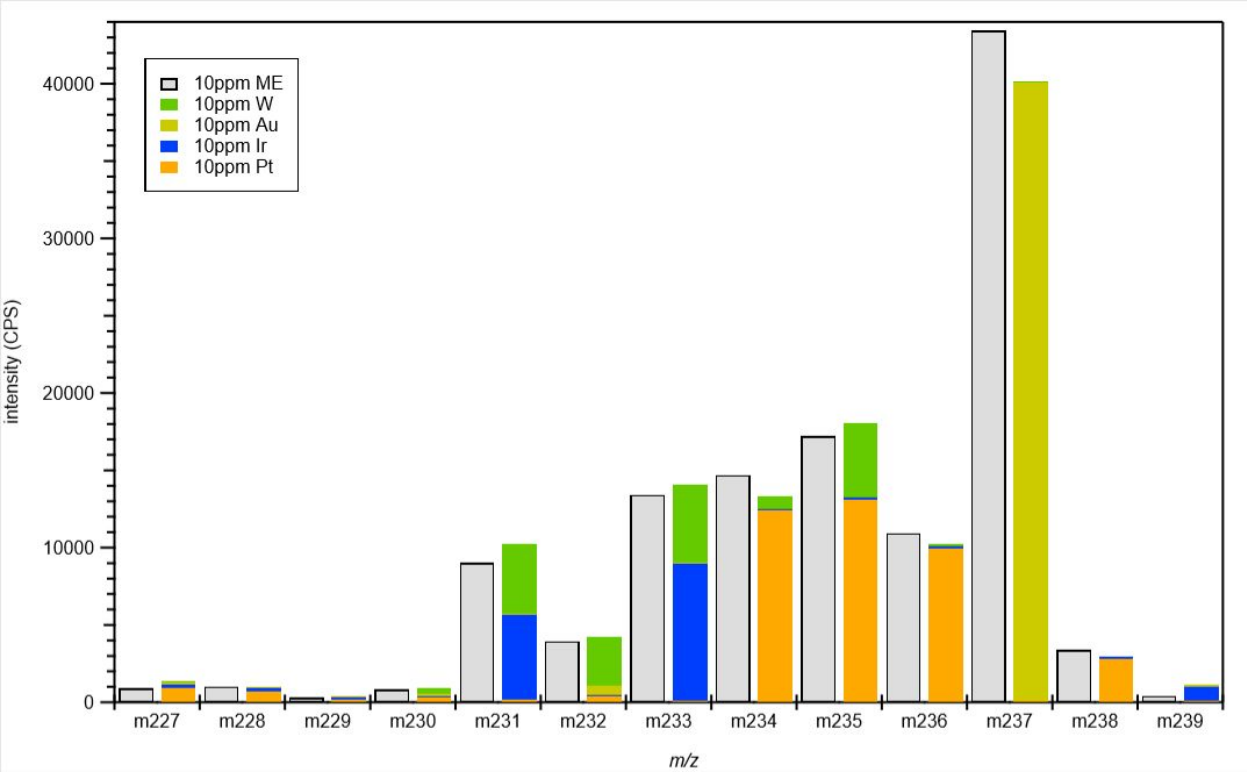

Figure 1. Matrix-derived interferences across *m/z* of 227 to 239 measured in single quad mode.

When operating in MS/MS mode, the overall signal intensity drops by roughly a factor of 3, as seen in (Fig. 2). The oxide interferences are not affected by the presence of O_2. While the argides of Pt and Au appear to react with O_2 to form argon oxide species, only the most abundant species are even detectable at *m/z* 250-253 with intensities of <10 cps (Fig. 2). The interference signals at *m/z* 250-253, and lack of signal at *m/z* 266-269 suggest that the formation of argon *monoxide* species is favored compared to the argon *dioxide* species.

Upon optimizing the instrument optics and reaction cell parameters for maximum oxide formation of U and Th species in the reaction cell, it was found that the monoxide for Th (ThO) and dioxide for U (UO_2) gave the highest intensity signal. It is unlikely that there are significant polyatomic interferences with our target analytes of ThO and UO_2. The main interferent on $^{229}Th^{16}O$ would be

$^{194}Pt^{35}Cl^{16}O$. However, it is not likely to have formed given the absence of signal at *m/z* 247 where the almost equally abundant $^{196}Pt^{35}Cl^{16}O$ species would be detected. Similarly, the main interference species on $^{232}Th^{16}O$ at *m/z* 248 would be $^{184}W^{16}O_4$, $^{183}W^{16}O_4H$, $^{197}Au^{35}Cl^{16}O$, $^{195}Pt^{37}Cl^{16}O$, and/or $^{192}Pt^{40}Ar^{16}O$. We can preclude the presence of tetraoxides of W due to the absence of signal at mass 247, which would correspond to the abundant species of $^{183}W^{16}O_4$ and $^{182}W^{16}O_4H$. The presence of $^{195}Pt^{37}Cl^{16}O$ overlapping with $^{232}Th^{16}O$ is also precluded by the absence of $^{196}Pt^{35}Cl^{16}O$ at *m/z* 247. While PtArO species are clearly formed on *m/z* 250-252, it is unlikely that $^{192}Pt^{40}Ar^{16}O$ is a significant interferent on $^{232}Th^{16}O$ as ^{192}Pt is a minor isotope of Pt (0.78% natural abundance) and the major PtArO species are only detectable at 5-6 cps. We cannot directly infer if the $^{197}Au^{35}Cl^{16}O$ species forms on *m/z* 248 by looking for $^{197}Au^{37}Cl^{16}O$ at *m/z* 250 due to overlap with $^{194}Pt^{40}Ar^{16}O$. We can, however, surmise that if it does form, it would be of a lower intensity than the more abundant $^{197}Au^{40}Ar^{16}O$, which forms at *m/z* 253 with an intensity of just 7 cps. Finally, we can also determine from the data that IrArO species do not form under our experimental conditions due to the absence of signal at *m/z* 247.

No signal was observed at *m/z* 266-269, which precludes the significant formation of any polyatomic dioxide interference species in the range of the UO_2 analytes. This result points to the clear advantage of employing a mass shift method where the analyte species is in the dioxide form when possible. The utility in measuring the dioxide of the analyte species is limited by commercial instrumentation and can therefore serve as incentive to the production of elemental instrumentation that can analyze up to an *m/z* of 275 or higher. This especially applies to all mass shift methods with analytes that react to form particularly large adducts when reacted with reactive gases (e.g., $BiCS_2$; (24))

We have demonstrated that the O_2 reaction gas method sufficiently removes overlapping polyatomic interferences from our analytes and is therefore a possible method for ultra-trace Th and U determinations. The following section addresses the viability of such an ultra-trace analysis.

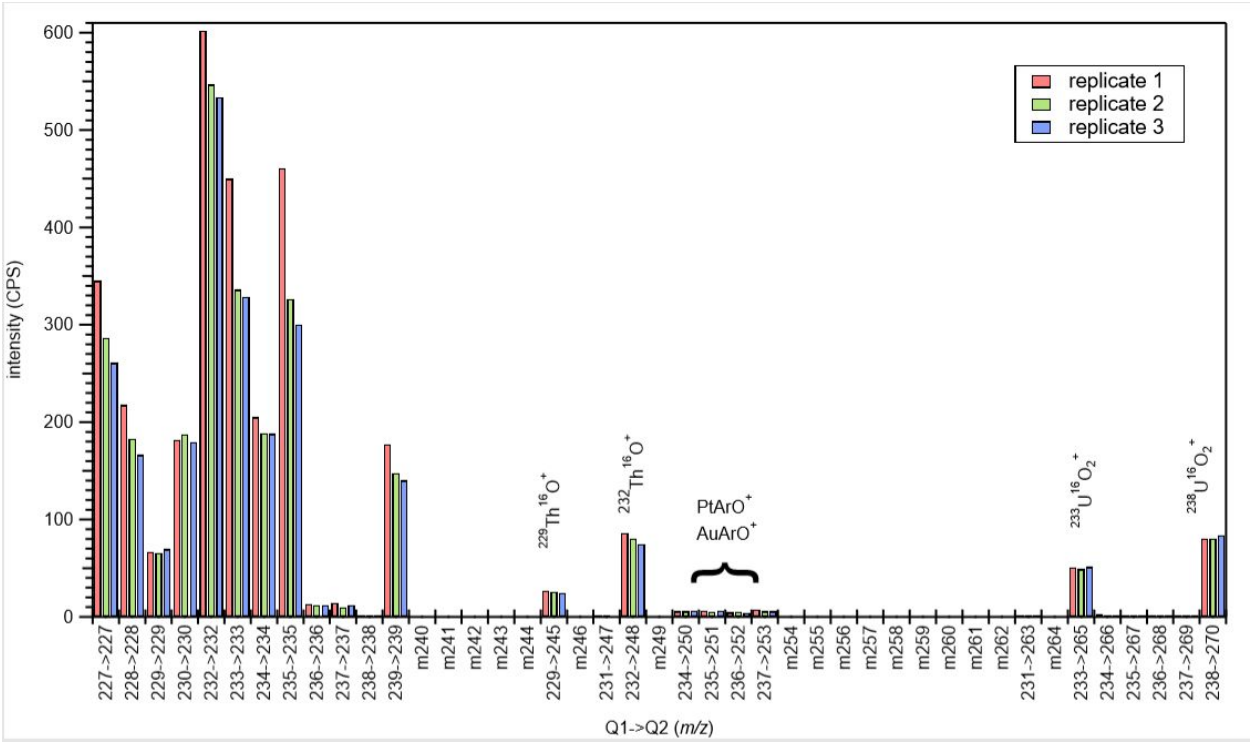

Figure 2. Signal intensities of the 10 µg·g^{-1} ME solution spiked with 100 fg·g^{-1} of ^{229}Th and ^{233}U tracer acquired in MS/MS mode. Signal was not acquired on the masses prefaced with an 'm' but are included in the graph to show the extent of the mass shift of the analytes.

3.2 Method detection limits and accuracy

Only the *m/z* of the monoxide of natural and synthetic Th and the dioxide of natural and synthetic U were acquired as they were confirmed to be the dominant reaction analyte species. Corresponding *m/z* to the isotopes of the species interfering with the analytes were also acquired (Table 1). The ME solution spiked with 100 fg·g^{-1} of ^{229}Th and ^{233}U was found to have an average of 3.06 ± 0.05 and 1.60 ± 0.03 pg·g^{-1} of ^{232}Th and ^{238}U, respectively (error is 1SD, n=3), which was used for the quantitation of the method accuracy analysis.

Table 3. Summary of the method accuracy analyses conducted in ME solutions using the natural isotopes of U and Th as the tracer.

sample[a]	^{229}Th (fg·g^{-1})		^{233}U (fg·g^{-1})	
	target	*measured*[b]	*target*	*measured*[b]

blanks				
Sp 0-1	0	0.4 ± 0.4	0	2.6 ± 1.2
Sp 0-2	0	0.1 ± 0.2	0	2.7 ± 0.4
Sp 0-3	0	0.1 ± 0.2	0	4.1 ± 1.7
blank subtracted samples				
Sp 1-1	0.989 ± 0.005	0.7 ± 0.8	1.09 ± 0.01	1.7 ± 1.2
Sp 1-2	1.15 ± 0.01	1.4 ± 0.5	1.26 ± 0.01	2.1 ± 1.3
Sp 1-3	1.14 ± 0.01	0.7 ± 0.9	1.25 ± 0.01	1.6 ± 1.2
Sp 10-1	11.6 ± 0.1	9.6 ± 1.7	12.8 ± 0.1	13.8 ± 1.8
Sp 10-2	11.6 ± 0.1	9.3 ± 1.8	12.8 ± 0.1	13 ± 2
Sp 10-3	11.6 ± 0.1	10.0 ± 1.6	12.8 ± 0.1	14.1 ± 1.8
Sp 100-1	101 ± 1	101 ± 6	101 ± 1	99 ± 4
Sp 100-2	101 ± 1	104 ± 4	101 ± 1	91 ± 3
Sp 100-3	100 ± 1	108 ± 6	100 ± 1	96 ± 4

a –Samples (or Sp) are labeled as Sp-x-y, where 'x' is the intended U and Th concentration and 'y' is the replicate number

b –The error is the standard deviation of a triplicate measurement

All measurements matched the target value within the 98% confidence limit. The method accuracy results indicate that the mass shift method can determine ^{229}Th measurements with 96% accuracy at 100 fg·g^{-1} levels, with 83% accuracy at 10 fg·g^{-1} levels, and with 73% accuracy at the 1 fg·g^{-1} concentration range. Similarly, ^{233}U can be measured with 95% accuracy at 100 fg·g^{-1} levels, with 94% accuracy at 10 fg g^{-1} levels, and with 51% accuracy at 1 fg·g^{-1} levels (Table 3). Our demonstration of the satisfactory removal of the relevant interference species (section 3.1) gives us a high degree of confidence with regards to the characterization of natural ^{232}Th and ^{238}U inherent to the ME solution and subsequent measurements of ^{229}Th and ^{233}U. The excellent reproducibility and accuracy of the measurements,

particularly at 10 $fg \cdot g^{-1}$ and above, show the viability of our mass shift method for challenging ultra-trace measurements.

The LOD using the ME matrix in this study was 3 and 13 fg of Th and U, respectively, which is about an order of magnitude higher than detection limits that are typically achievable in 2% HNO_3 blank solutions measured in single quad mode with our instrument. While the U signal had a higher sensitivity, the Th signal had better short-term stability (*i.e.,* had smaller deviations between replicate measurements) and therefore had lower LODs. Our method accuracy and detection limit results are specific to a coinage metal background of 10 $\mu g \cdot g^{-1}$. Given the propensity for metals such as Au, Pt, Ir, and W to create carryover effects in the instrument, it is not desirable to measure solutions with coinage metal matrices greater than 10 $\mu g \cdot g^{-1}$. In many electronic components such as ASICs, SiPMs, capacitors, diodes, PCBs, resistors, and SQUID arrays, the coinage metal content is mainly contained within coatings or electrical contacts that often make up ≤0.1% of the total weight *e.g.*, (14,16,25). Assuming a 1 g sample has 1 mg of coinage metal content, dilution down to 10 µg coinage metals·g sample $solution^{-1}$ via our method would yield detection limits of 300 and 1300 fg of Th and U, respectively. It is useful to note that the complete digestion of an electronic sample with minor amounts of coinage metals typically involves use of HNO_3, HCl, and HF, which involves multiple dry down steps in order for the final measured solution to have a matrix of 2% HNO_3. It is, therefore, feasible to reduce the dissolved coinage metal content during the dry down steps through precipitation when using an isotopic tracer, which would limit the need for dilution and improve the detection limits (table 4). This could also enable the measurement of samples with a much greater coinage metal content, or even solid metal samples, with similar detection limits. Examples of such analyses are described in the following section.

3.3 Determination of U and Th in electronic samples

The O_2 mass shift method was applied to determine U and Th concentrations in commercially available electronic components for the MAJORANA/LEGEND, nEXO, and SuperCDMS physics

collaborations (1–3). Samples include board mounts and crimps (Axon' Cable; Montmirail, France), gold bonding wire (Ametek Inc; Berwyn, PA), and superconducting quantum interference device (SQUID) arrays (fabricated by NIST; Boulder, CO). All the samples contain proprietary concentrations of some or all of the coinage metal interferants with U and Th: The Axon' board mount and crimps contain some quantity of Au and other precious metals. The bonding wire is made of gold and the NIST fabricated SQUIDs contained ~1-5 wt% Au as well as trace amounts of W, Pt and Ir.

The samples were spiked with the synthetic ^{229}Th and ^{233}U tracer and digested in a mixture of concentrated acids (Optima grade nitric acid, hydrochloric acid, hydrofluoric acid) either at room temperature, or in a microwave digestion system (Mars 6; CEM corporation, Charlotte, NC)) as needed. Aliquots of the digested samples were diluted/resuspended in 2% HNO_3 as necessary and analysed following the O_2 mass shift method described above. The ^{232}Th and ^{238}U concentrations were determined following isotope dilution methods (eqn. 1). The results of the measurements are reported in table 4.

Table 4. U and Th content of various electronic samples as determined using the O_2 mass shift method

sample	replicate	weight (g)	^{232}Th (pg·g^{-1})	LOD (pg·g^{-1})	^{238}U (pg·g^{-1})	LOD (pg·g^{-1})
direct crimp (Axon'Cable)	1	0.3142	35 ± 7	5	41 ± 5	1
	2	0.2945	63 ± 8	6	56 ± 7	1
board mount (Axon'Cable)	1	0.1873	99 ± 10	10	120 ± 11	2
gold bonding wire (Ametek Inc)	1	0.0997	18 ± 14	17	52 ± 6	8
	2	0.2295	27 ± 7	7	190 ± 15	3
	3	0.2572	34 ± 5	7	54 ± 8	3
SQUID arrays (NIST)	1	0.0162	12.8 ± 0.7	1	9.9 ± 1.0	2
	2	0.0173	14.1 ± 0.7	1	8.6 ± 0.9	1
	3	0.0155	19 ± 2	1	15 ± 2	2

4. **Conclusions**

The work in this study demonstrates a novel method for the determination of fg·g^{-1} levels of U and Th in a matrix of Au, Pt, Ir, and W. The method employs an O_2 reaction gas to produce analyte ions of

interest free from or with minor contributions from polyatomic interferences. Some of the polyatomic interferences produced by the matrix elements were shown to form oxides at intensities that were too low to cause a significant interference with the target masses. The polyatomic interferences at *m/z* of 234-237 that formed monoxide species at *m/z* of 250-253 did not form dioxide species at *m/z* 266-269. The technique was able to measure standards solutions as low as 10 $fg \cdot g^{-1}$ with >80% accuracy.

The method is valuable because it provides a simple and convenient alternative for the measurement of ultra-trace U and Th in coinage metal matrices for which no viable chemical separation exists. This method will allow the high energy and nuclear physics communities to meet the growing demand for lower thresholds of radio contaminants in components with challenging matrices (e.g., electronics). This method may also allow us to revisit the electrowinning technique to assay ultra-pure electroformed copper using Ir electrodes, where, prior to this method, Ir contamination at concentrations 10^5 times greater than the inherent U made the ultra-trace assay untenable (Matthews et al., 2016). Finally, this method will also be useful to other fields of research, such as the semiconductor industries where ultra-low levels of radio-contaminants are also of increasing importance *e.g.,* (17).

Acknowledgements:

The authors acknowledge standard procurement assistance from May-Lin Thomas at PNNL. The authors also acknowledge assay samples provided by the following high energy physics and nuclear physics collaborations: MAJORANA, LEGEND, nEXO, and SuperCDMS. The Axon' samples were supplied by Matthew Busch (MAJORANA/LEGEND), the bonding wire was supplied by Dave Moore (nEXO) and the SQUIDs were supplied by Bruce Hines (SuperCDMS). The preparation of the manuscript has benefited from the review of two anonymous reviewers. This work was funded by PNNL Laboratory Directed Research and Development funds under the Nuclear Physics, Particle Physics, Astrophysics, and Cosmology Initiative. The Pacific Northwest National Laboratory is a multi-program national laboratory operated for the U.S. Department of Energy (DOE) by Battelle Memorial Institute under contract number DE-AC05-76RL01830.

References:

1. Albert JB, Auty DJ, Barbeau PS, Beauchamp E, Beck D, Belov V, et al. Search for Majorana neutrinos with the first two years of EXO-200 data. Nature [Internet]. 2014 Jun 1 [cited 2020 Sep 18];510(7504):229–34. Available from: https://www.nature.com/articles/nature13432

2. Agnese R, Aralis T, Aramaki T, Arnquist IJ, Azadbakht E, Baker W, et al. First Dark Matter Constraints from a SuperCDMS Single-Charge Sensitive Detector. Phys Rev Lett [Internet]. 2018

Aug 3 [cited 2020 Sep 18];121(5):51301. Available from: https://journals.aps.org/prl/abstract/10.1103/PhysRevLett.121.051301

3. Alvis SI, Arnquist IJ, Avignone FT, Barabash AS, Barton CJ, Bertrand FE, et al. First Limit on the Direct Detection of Lightly Ionizing Particles for Electric Charge as Low as e/1000 with the Majorana Demonstrator. Phys Rev Lett [Internet]. 2018 May 25 [cited 2020 Sep 18];120(21):211804. Available from: https://journals.aps.org/prl/abstract/10.1103/PhysRevLett.120.211804

4. Arpesella C, Back HO, Balata M, Beau T, Bellini G, Benziger J, et al. Measurements of extremely low radioactivity levels in BOREXINO. Astropart Phys. 2002 Aug 1;18(1):1–25.

5. Leonard DS, Grinberg P, Weber P, Baussan E, Djurcic Z, Keefer G, et al. Systematic study of trace radioactive impurities in candidate construction materials for EXO-200. Nucl Instruments Methods Phys Res Sect A Accel Spectrometers, Detect Assoc Equip. 2008 Jul 1;591(3):490–509.

6. Aprile E, Arisaka K, Arneodo F, Askin A, Baudis L, Behrens A, et al. Material screening and selection for XENON100. Astropart Phys. 2011 Sep 1;35(2):43–9.

7. GERDA Collaboration, Agostini M, Allardt M, Bakalyarov AM, Balata M, Barabanov I, et al. Improvement of the energy resolution via an optimized digital signal processing in GERDA Phase I. Eur Phys J C [Internet]. 2015 Jun 10 [cited 2020 Sep 18];75(6):23. Available from: https://link.springer.com/article/10.1140/epjc/s10052-015-3409-6

8. Cebrián S, Pérez J, Bandac I, Labarga L, Álvarez V, Barrado AI, et al. Radiopurity assessment of the tracking readout for the NEXT double beta decay experiment. J Instrum [Internet]. 2015 May 1 [cited 2020 Sep 18];10(5):P05006. Available from: https://iopscience.iop.org/article/10.1088/1748-0221/10/05/P05006

9. Arnquist IJ, Hoppe EW. The quick and ultrasensitive determination of K in NaI using inductively coupled plasma mass spectrometry. Nucl Instruments Methods Phys Res Sect A Accel Spectrometers, Detect Assoc Equip. 2017 Apr 11;851:15–9.

10. Arnquist IJ, Beck C, di Vacri ML, Harouaka K, Saldanha R. Ultra-low radioactivity Kapton and copper-Kapton laminates. Nucl Instruments Methods Phys Res Sect A Accel Spectrometers, Detect Assoc Equip. 2020 Apr 11;959:163573.

11. Laferriere BD, Maiti TC, Arnquist IJ, Hoppe EW. A novel assay method for the trace determination of Th and U in copper and lead using inductively coupled plasma mass spectrometry. Nucl Instruments Methods Phys Res Sect A Accel Spectrometers, Detect Assoc Equip. 2015 Mar 1;775:93–8.

12. Arnquist IJ, Hoppe EJ, Bliss M, Grate JW. Mass Spectrometric Determination of Uranium and Thorium in High Radiopurity Polymers Using Ultra Low Background Electroformed Copper Crucibles for Dry Ashing. Anal Chem [Internet]. 2017 Mar 7 [cited 2020 Sep 18];89(5):3101–7. Available from: https://pubs.acs.org/sharingguidelines

13. Arnquist IJ, Hoppe EW, Bliss M, Harouaka K, di Vacri ML, Grate JW. Mass spectrometric assay of high radiopurity solid polymer materials for parts in radiation and rare event physics detectors. Nucl Instruments Methods Phys Res Sect A Accel Spectrometers, Detect Assoc Equip. 2019 Nov 1;943:162443.

14. Ness M Van. Proceedings of the mineral waste utilization symposium, 7th: mining and mineral processing waste-urban solid waste-industrial waste recovery-scrap metal recovery. osti.gov [Internet]. [cited 2020 Sep 18]; Available from: https://www.osti.gov/biblio/6529040

15. McDonald D, Hunt L. A history of platinum and its allied metals [Internet]. 1982 [cited 2020 Sep 18]. Available from: https://books.google.com/books?hl=en&lr=&id=xriMAgAAQBAJ&oi=fnd&pg=PP5&dq=McDonald,+D.+and+Hunt,+L.B.,+1982.+A+history+of+platinum+and+its+allied+metals.+Johnson+Matthey+Plc

.&ots=FMuEvkc6yN&sig=BL5mHh1t1V6MR_2u9bkz-cNSxRY

16. Işildar A. Metal Recovery from Electronic Waste: Biological Versus Chemical Leaching for Recovery of Copper and Gold [Internet]. 2018 [cited 2020 Sep 18]. Available from: https://books.google.com/books?hl=en&lr=&id=wZV2DwAAQBAJ&oi=fnd&pg=PR4&dq=Işildar,+A.,+2018.+Metal+Recovery+from+Electronic+Waste:+Biological+Versus+Chemical+Leaching+for+Recovery+of+Copper+and+Gold.+CRC+press.&ots=Jd3Rqh3UxV&sig=m7_MBzOAxD3Z5YsxkPB8SCMfOfg

17. Gordon MS, Rodbell KP, Murray CE, McNally BD. Measurements of radioactive contaminants in semiconductor materials [Internet]. Vol. 31, Semiconductor Science and Technology. Institute of Physics Publishing; 2016 [cited 2020 Sep 18]. p. 123003. Available from: https://iopscience.iop.org/article/10.1088/0268-1242/31/12/123003

18. Mathews M, LaFerriere BD, Pederson LR, Hoppe EW. Plating of iridium for use as high purity electrodes in the assay of ultrapure copper. J Radioanal Nucl Chem [Internet]. 2016 [cited 2020 Sep 18];307(3):2577–85. Available from: https://link.springer.com/content/pdf/10.1007/s10967-016-4697-5.pdf

19. Ichikawa F, Uruno S, Imai H. Distribution of Various Elements between Nitric Acid and Anion Exchange Resin. Bull Chem Soc Jpn [Internet]. 1961 Jul 12 [cited 2020 Sep 18];34(7):952–5. Available from: https://www.journal.csj.jp/doi/abs/10.1246/bcsj.34.952

20. Faris JP, Buchanan RF. Anion Exchange Characteristics of the Elements in Nitric Acid Medium [Internet]. Vol. 36, Analytical Chemistry. Wiley; 1964 [cited 2020 Sep 18]. p. 1157–8. Available from: https://pubs.acs.org/sharingguidelines

21. Pourmand A, Dauphas N. Distribution coefficients of 60 elements on TODGA resin: Application to Ca, Lu, Hf, U and Th isotope geochemistry. Talanta. 2010 May 15;81(3):741–53.

22. Maxwell SL, Culligan BK, Noyes GW. Rapid separation of actinides and radiostrontium in vegetation samples. J Radioanal Nucl Chem. 2010 Oct;286(1):273–82.

23. McNaught A, Wilkinson A. Compendium of chemical terminology. IUPAC recommendations. 1997 [cited 2020 Sep 18]; Available from: http://agris.fao.org/agris-search/search.do?recordID=XF2015028589

24. Cheng P, Koyanagi GK, Bohme DK. Carbon disulfide reactions with atomic transition-metal and main-group cations: Gas-phase room-temperature kinetics and periodicities in reactivity. J Phys Chem A [Internet]. 2006 Mar 2 [cited 2020 Sep 18];110(8):2718–28. Available from: https://pubs.acs.org/sharingguidelines

25. Szałatkiewicz J. Metals content in printed circuit board waste. Polish J Environ Stud [Internet]. 2014 [cited 2020 Sep 18];23(6):2365–9. Available from: https://www.academia.edu/download/36855456/Pol.J.Environ.Stud.Vol.23.No.6.2365-2369.pdf